Trans. JSASS Aerospace Tech. Japan
Vol. 18, No. 3, pp. 25-31, 2020
DOI: 10.2322/tastj.18.25

Deployment Repeatability of Pointing Performance for Highly Precise Extensible Optical Bench Considering Uncertainties on Backlash and Friction

By Yoya GON[1)] and Nozomu KOGISO[1)]

[1)]*Department of Aerospace Engineering, Osaka Prefecture University, Sakai, Japan*

(Received July 9th, 2019)

The authors have investigated the effects of uncertainties on the pointing performance of an extensible optical bench (EOB), used for a large, highly precise, space X-ray telescope. The uncertainties considered are in member length, position due to backlash, and friction at connecting nodes. This study mainly investigates the effect of friction on the pointing performance. First, the pointing performance analysis is briefly investigated. The extended EOB is modeled as a truss structure, and the distortion due to the member length imperfection is evaluated by a nonlinear, finite element analysis (FEA). Subsequently, the backlash at connecting nodes is modeled by introducing a virtual cable element with a natural length equal to the size of backlash. In addition, the deformation due to a friction force acting at the connecting node is calculated as a perturbation from the equilibrium condition without performing a contact analysis. This friction model is further extended to identify effects of friction uncertainty with reduced computational costs. Through numerical examples, the effects of friction uncertainty on the deployment repeatability for the EOB, and effects of the number of stages of EOB on the pointing performance are investigated.

Key Words: Extensible Optical Bench, Uncertainty, Pointing Performance, Backlash, Friction

1. Introduction

This study investigates effects of uncertainties on the pointing performance of a deployable (extensible) optical bench that is a component of a large space optical system developed for an astronomy mission. At a highly precise space observatory, a space X-ray telescope requires a longer focal length than the length of a launch vehicle fairing. Therefore, an extensible optical bench (EOB), which is stored in the fairing of the launch vehicle and deployed in orbit, was developed for a hard X-ray telescope on HITOMI (Astro-H). This spacecraft was launched in 2016 and is shown in Fig. 1. The hard X-ray telescope has a 12 m focal length. This EOB with a 6 m length can be folded to store into the fairing of H-IIA, and a fixed optical bench (FOB) with a 6 m length is stored with its shape.[1)] The pointing accuracy requirement for the hard X-ray telescope on HITOMI was less than 69 arcseconds.[2)]

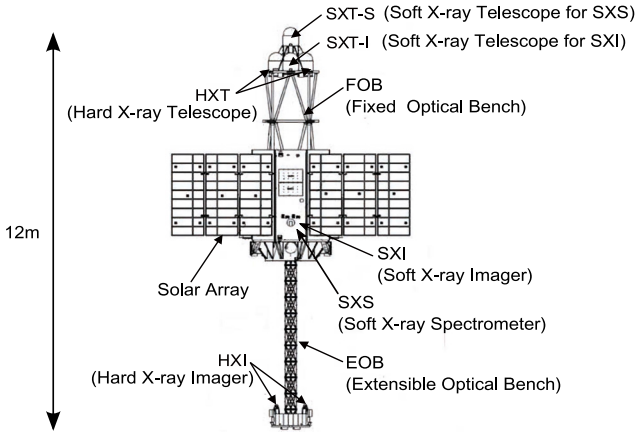

Fig. 1. Overview of HITOMI (Astro-H).[2)]

In future space astronomy missions, the pointing accuracy requirement for the optical bench will be strictly reduced to the order of arcseconds. FORCE (FOcusing Relative universe and Cosmic Evolution) is a planned mission involving a small satellite for X-ray astronomy observation. It will explore an undiscovered black hole in each stratum to elucidate the early universe. This mission will observe an active galactic nucleus via hard X-ray imaging spectroscopy with more than 10 keV power and more than 10 times the spatial resolution than those of conventional observation techniques.[3,4)] The X-ray telescope used in FORCE has more than a 10 m length and is composed of a next-generation EOB and FOB. Its pointing accuracy requirement will be extremely low: 5 arcsec for the attitude determination requirement. The pointing accuracy requirement for this next-generation EOB will be as strictly set as 1 arcsec with active control.[5)] This requirement is extremely precise in comparison to that of 69 arcsec by HITOMI. Considering the control performance, the pointing accuracy requirement for the EOB itself will be 20 arcsec, sufficient to distinguish a 1 mm distance up to 10 m in front of the satellite.

Both of the EOB on HITOMI and the next-generation EOB on FORCE are designed as a one-dimensional, deployable, structural system along the optical axis. The deployment mechanism will sacrifice pointing accuracy due to backlash at the connecting nodes of the components. In addition, the member length uncertainty due to manufacturing tolerance will affect the pointing accuracy.

This study extends previous studies that have sought to examine the same effects of uncertainty.[6–8)] The friction in this study is modeled as a couple force equivalent to the moment acting through the connecting nodes. Uncertainty of the friction force is modeled by considering the variability of the static friction coefficient at the connecting node. First, the effect of the friction on the pointing direction is clarified through two mod-

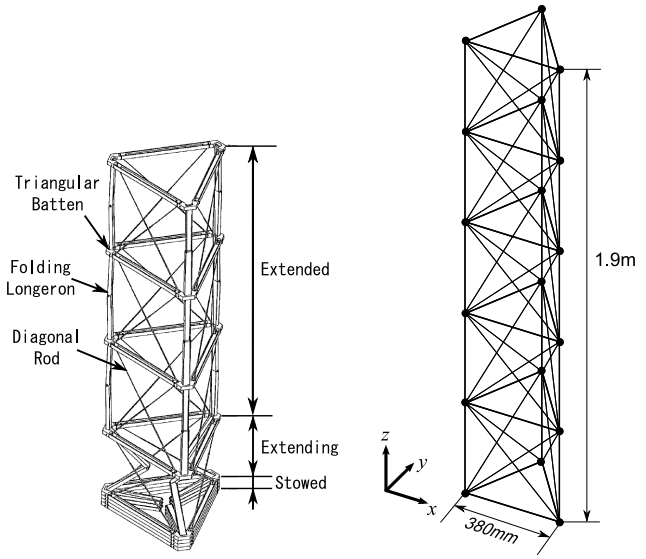

(a) EOB.[9] (b) Analysis model.

Fig. 2. EOB structure and analysis model.

els; a simple two-dimensional and a five-stage EOB model that have huge backlash at each connecting nodes. These models are used to demonstrate the potential for uncertainty. Then, the effects of friction uncertainty on deployment repeatability for the EOB and the number of stages of the EOB on the pointing performance are investigated.

2. Analysis Model of Extended Optical Bench (EOB)

2.1. Structural analysis model

The deployment behavior of the EOB on HITOMI is shown in Fig. 2(a).[9] This EOB is composed of a 23-stage truss, and the total height of this EOB is only 689 mm when stored in the launcher. It is deployed to 6377 mm in orbit by sequentially extending the stages from the tip.[10] Each stage is composed of three main components: triangular battens, folding longerons, and diagonal rods, which are tension members with variable lengths.

An example of the structural analysis model of the deployed EOB with five stages is shown in Fig. 2(b). The longerons and battens are made of aluminum cylinders of diameter 10 mm and thickness 1 mm. The diagonal rods are composed of aluminum cables with a diameter of 2 mm. These are assumed to support only the tension force. Therefore, the stiffness is set as zero for the compression load. Because a pair of completely folded longerons is extended to a straight shape after deployment, it was modeled as a single truss member. In addition, because each node is connected by a shaft, they can move only in the direction perpendicular to the shaft. The material properties of the members are listed in Table 1.

2.2. Pointing analysis

The deployed EOB is intrinsically deployed straight along the optical axis. However, several uncertainties, such as member length, backlash, and friction at the nodes, distort the deployment direction of the EOB. As the distorted state can be obtained from an equilibrium condition due to the uncertainties, the distortion of the EOB was calculated by using a nonlinear, finite element method. The equilibrium equation is described

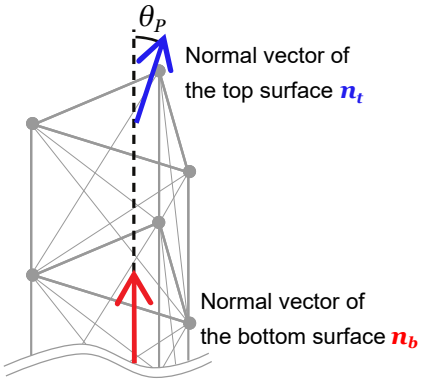

Fig. 3. Definition of the pointing direction, θ_P.

as follows:[11]

$$\boldsymbol{F}^e + \boldsymbol{f}^e = \boldsymbol{K}^e \boldsymbol{d}^e. \tag{1}$$

In Eq. (1), $\boldsymbol{F}^e$ is the nodal force vector, $\boldsymbol{K}^e$ is the element stiffness matrix, $\boldsymbol{d}^e$ is the nodal displacement vector, and $\boldsymbol{f}^e$ is the initial nodal force vector. The initial nodal force was evaluated as the resultant force of all the initial axial forces resulting from the length imperfection. Equation (1) was solved by using Newton's method.[12] Then, the pointing performance was evaluated as the angle formed by $\boldsymbol{n}_b$, the normal vector of the bottom surface of the truss, and $\boldsymbol{n}_t$, the normal vector of the top surface, as shown in Fig. 3. The distortion angle, θ_P, is evaluated from the following equation:

$$\theta_P = \cos^{-1} \frac{\boldsymbol{n}_t^{\mathrm{T}} \boldsymbol{n}_b}{|\boldsymbol{n}_t||\boldsymbol{n}_b|}. \tag{2}$$

In this study, the target pointing accuracy is assumed as $\theta_P \leq 20$ arcsec.

2.3. Backlash model

At the connecting node, a sliding part is required for deploying and folding the EOB.[13] However, this sliding part causes uncertainty of node position, resulting in additional uncertainty in the pointing direction.

As shown in Fig. 4(a), a batten is connected to a longeron at the connecting node by fitting a shaft into a hole on the longeron. The shaft diameter should be slightly smaller than the hole diameter for insertion. However, that causes backlash at the connecting node. The backlash was modeled by introducing a virtual cable element to connect the ends of a batten and a longeron as shown in Fig. 4(b), where both end nodes are located at the centers of the shaft and the hole, respectively. The length of the cable element was set equal to the difference of diameters of the hole and the shaft. To model the backlash, stiffness of the cable element was set to infinity at the tensile side and zero at the compression side. A simple two-dimensional truss model with backlashes was considered in Fig. 5. The truss was composed of four truss members on each side of 380 mm length and two diagonal rods. The four corners assumed backlashes as large as 30 mm to demonstrate effects. The backlashes were modeled by virtual cable elements.

To eliminate the backlash, the diagonal rods were shortened from 537 mm to 445 mm, where the member failure including buckling were ignored. The stiffness of the virtual cable elements at the tensile side was set to 10^3 times higher than other members. Then, the equilibrium state was evaluated by using

Table 1. Member specifications of EOB for structural analysis, where all members are made of Al alloy.

	Triangular batten	Folding longeron	Diagonal rod	
			Tension	Compression
Natural length [mm]	380	380	537.4	537.4
Cross sectional area [mm^2]	14.9	14.9	3.1	3.1
Young's modulus [GPa]	70	70	70	0

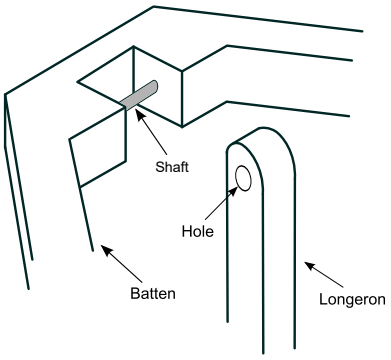

(a) Backlash caused by a hole of longeron and a shaft of batten at the connecting node.

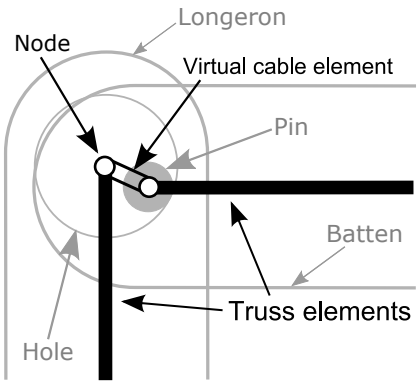

(b) Virtual cable element describing backlash uncertainty for structural analysis.

Fig. 4. Backlash uncertainty at a connecting node.

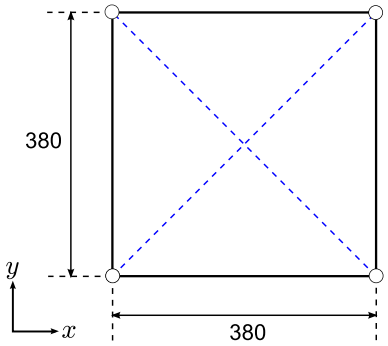

Fig. 5. Two-dimensional one-stage truss structure model.

structural analysis at the fixed, lower batten nodes. The equilibrium state is shown in Fig. 6(a), and the extended view around the upper left node is shown in Fig. 6(b). It was found that the longeron is tilted when eliminating backlash.

2.4. Friction model

Friction force generated at the contact surface between the hole in the longeron and the shaft of the batten works as a virtual reaction moment M at the center of the hole, as shown in the left hand side of Fig. 7. Since the virtual cable element cannot support a moment, friction force was modeled as an equivalent

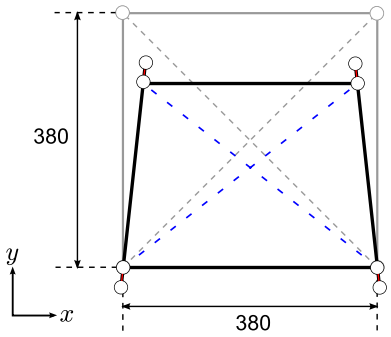

(a) Equilibrium state.

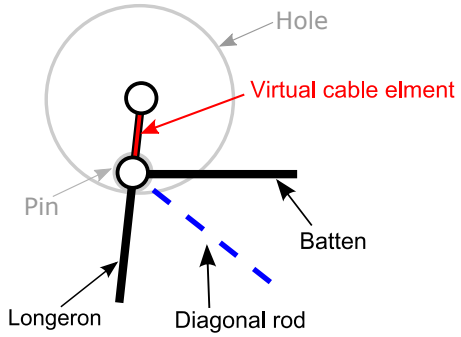

(b) Expansion view of around the upper left node.

Fig. 6. Two-dimension truss structure model with large backlashes in actual size (the length of diagonal rods shortened to 445 mm, backlash size: 30mm at each node).

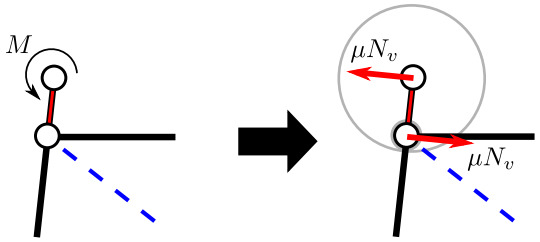

Fig. 7. Couple of forces equivalent to virtual friction moment that inhibits deployment.

couple force as P_c as shown in the right-hand side of Fig. 7 to enable analysis as a truss structure. The magnitude of P_c was obtained by the following equation.

$$P_c = \mu N_v, \tag{3}$$

where μ and N_v indicate a static friction coefficient and axial force of the virtual cable element, respectively. Here, N_v is equivalent to the normal force that the shaft receives from the hole. The static friction coefficient μ is described as $\mu = f/N_v = F/N_v$ in equilibrium state where f is the static friction force and F is the member axial force on the node. The direction of the couple force $\boldsymbol{t}_c$ was set orthogonal to the virtual cable element.

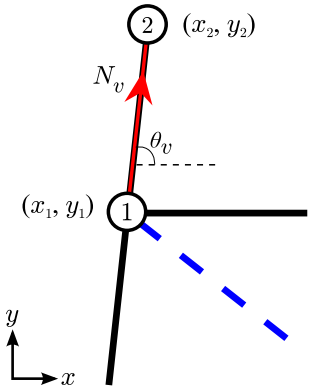

Fig. 8. Definition of node coordinates.

2.5. Pointing analysis flow considering uncertainties

First, the node coordinates $\boldsymbol{d}$ were calculated without considering the friction using a nonlinear, finite element method. Secondly, the magnitude and direction of the couple force P_c shown in Fig. 7 was calculated from the node coordinates, the axial force of the virtual cable element N_v and friction coefficient μ. The magnitude of the couple force P_c was obtained by Eq. 3.

The direction of the couple force was set equal to the tangential direction of the hole in the longeron, orthogonal to the virtual cable element. The direction vector of the virtual cable member $\boldsymbol{t}_v$ at the shaft center node of the batten is written as follows:

$$\boldsymbol{t}_v = (\cos\theta_v, \sin\theta_v) = \left(\frac{x_2 - x_1}{L_v}, \frac{y_2 - y_1}{L_v}\right). \tag{4}$$

Here, (x_1, y_1) are the nodal coordinates of shaft center of the batten (node 1) and (x_2, y_2) represents the hole center of the longeron (node 2). $L_v = \sqrt{(x_2 - x_1)^2 + (y_2 - y_1)^2}$ is the length of the virtual cable element and θ_v is the angle between the virtual cable element and the x axis.

The direction vector of the couple force at the shaft center of the batten (node 1) is either $\boldsymbol{t}_{c1} = (-\sin\theta_v, \cos\theta_v)$ or $(\sin\theta_v, -\cos\theta_v)$. When the longeron (node 2) is located above the batten (node 1), $\boldsymbol{t}_{c1} = (\sin\theta_v, -\cos\theta_v)$ is used. When the batten (node 1) is located above the longeron (node 2), $\boldsymbol{t}_{c1} = (-\sin\theta_v, \cos\theta_v)$ is used.

A couple force equivalent to the friction moment was applied at both of the end nodes of the virtual cable element. The force with magnitude P_c in the direction of $\boldsymbol{t}_{c1}$ was applied to the shaft center of the batten (node 1), and the force with magnitude P_c in the direction of $\boldsymbol{t}_{c2} = -\boldsymbol{t}_{c1}$ was applied to the hole center of the longeron (node 2). Then, the node position $\boldsymbol{d}$ was obtained by applying a nonlinear, finite element method, and the magnitude of the couple force P_c and the direction $\boldsymbol{t}_{c1}, \boldsymbol{t}_{c2}$ were updated from the coordinates. This calculation was repeated until reaching the convergence of the pointing direction, θ_P. The flowchart of this pointing analysis is shown in Fig. 9.

Finally, the uncertainty of friction is explained. The maximum static friction force f_0 at a node is given by $f_0 = \mu_0 N_v$ where μ_0 is the maximum static friction coefficient. The static friction force f can take any value less than f_0 in real-life conditions. The friction coefficient μ was assumed to follow uniform distribution of $[-\mu_0, \mu_0]$ because the friction force f may work in any direction.

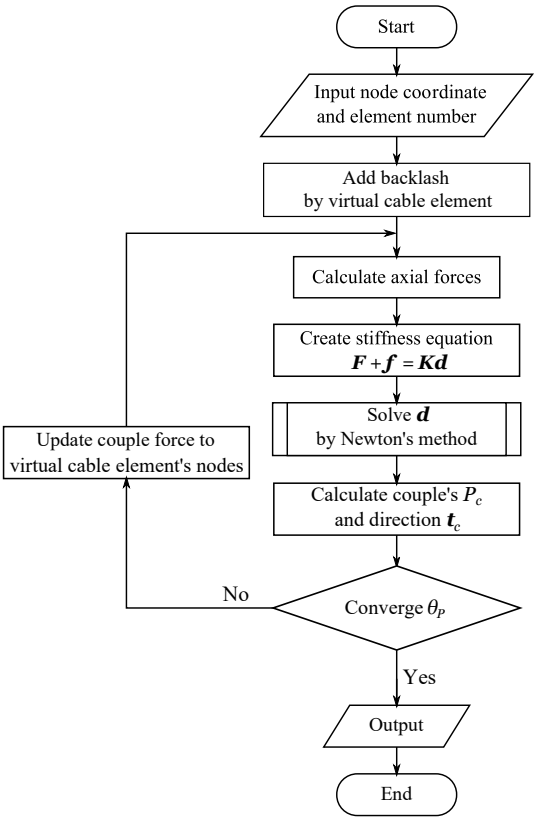

Fig. 9. Flowchart of analysis with friction.

There are three parameters related to friction: $F(=f)$, N_v, and μ. However, since $F(=f)$ and N_v are determined by the equilibrium condition of the structure, they are greatly affected by the uncertainty of member length and backlash size. On the other hand, since μ is not affected by these uncertainties, it is most appropriate parameter for modeling friction uncertainty.

3. Structure Analysis of a Simple Truss Model Considering Backlash and Friction

In this section, the validity of the friction model is investigated using two simple structural models.

3.1. A simple two-dimensional model

The proposed friction model was applied to a two-dimensional, one-stage truss model shown in Fig. 5. For simplicity, friction was considered only at the two nodes on the top side, and the friction coefficient was taken as a constant: the maximum static friction coefficient $\mu_0 = 0.57$[14] which is used for friction between Al alloy members.

The deformation shapes with and without considering the friction are shown as black and light gray in Fig. 10, respectively. When the friction was not considered, the shaft center of the batten was located in the axial direction of the longeron. When the friction was considered, however, the shaft center of the longeron was not aligned with the axial direction of the longeron due to the friction force between the hole of the longeron and the shaft of the batten.

3.2. Three-dimensional EOB model

The effect of friction was investigated for the three-dimensional, five-stage EOB model shown in Fig. 2(b). In this

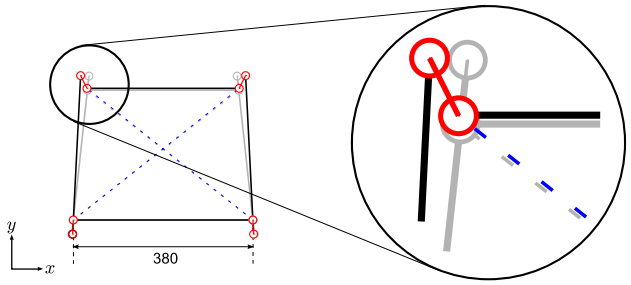

Fig. 10. Effect of friction at connecting nodes on the deformation shape of a two-dimensional one-stage truss model.

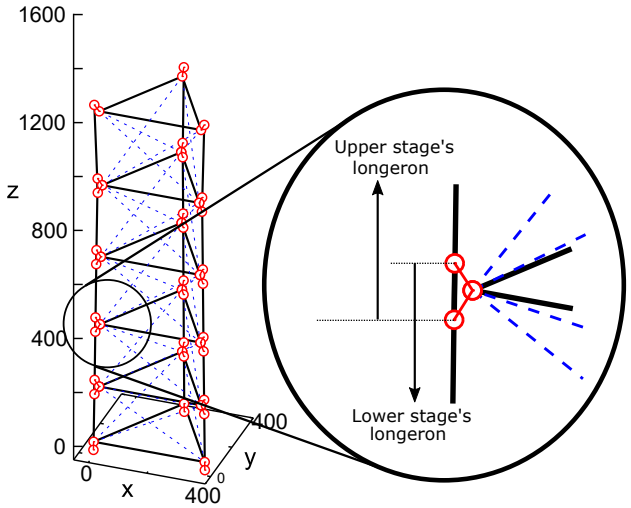

Fig. 11. Considering friction to the five-stage EOB model in actual size (the length of diagonal rods shortened to 445 mm, backlash size: 30mm at each node).

model, all of the connecting nodes were assumed to have large backlashes of 30 mm to demonstrate the effects. The virtual cable elements and the end nodes are indicated with a red color in Fig. 11. To eliminate the backlash, the diagonal rods were shortened from 537 mm to 445 mm. The stiffness of the virtual cable elements at the tensile side was set to 10^3 times higher than other members, the same as the two-dimensional model. The friction was considered at all the nodes except for the bottom three at the base. The friction coefficient was taken as a constant $\mu_0 = 0.57$, the same as the two-dimensional model. The direction of the couple force depends on the relative position of the longeron and the batten. In three-dimensional model, it was assumed that the hole does not tilt to the shaft. That is, the hole can only be translated in the direction perpendicular to the shaft.

The deformation of the three-dimensional model had the same tendency as that of the simple two-dimensional model described in the previous subsection. It should be noted that the upper and lower stage's longerons are only connected to the batten by virtual cable elements. They are drawn overlapping in Fig. 11, but they are not connected. In addition, it was found that the EOB structure cannot be perfectly deployed and the overall height was lowered due to the friction force acting in the direction as shown in Fig. 12. The deformation shapes with and without considering the friction are shown as black and light gray, respectively.

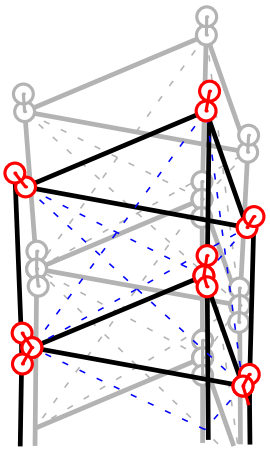

Fig. 12. Deformation shape around top surface for the five-stage EOB model considering friction in actual size (the length of diagonal rods shortened to 445 mm, backlash size: 30mm at each node).

4. Pointing Performance Considering Friction Uncertainty

4.1. Analysis of five-stage model

An effect of the friction uncertainty on the pointing performance was investigated by using the five-stage EOB shown in Fig. 2(b). The friction uncertainty affected all of the nodes except for the fixed nodes at the bottom surface, where the friction coefficient was assumed to have uncertainty that follows the following three types of probabilistic distributions. The first case (case 1) was set as a uniform distribution of [-0.57, 0.57]. The second (case 2) was set as a truncated normal distribution $N(0, \sigma_1^2)$ with an interval [-0.57, 0.57] where $\sigma_1 = 0.57/\sqrt{3}$. This standard deviation σ_1 was the same as case 1, with uniform distribution. The last case (case 3) was set as a truncated normal distribution $N(0, \sigma_2^2)$ of [-0.57, 0.57] where $\sigma_2 = 0.57/3$. The pointing performance was evaluated by Monte Carlo simulation with 10000 samples.

In this study, backlash was given to all nodes with a size of 0.01 mm without uncertainty and the member length uncertainty was ignored. To eliminate the backlash, the diagonal rods were shortened 0.3 mm, which is large enough for the backlash size 0.01 mm. Therefore, all of the backlashes are eliminated in any friction uncertainty. The pointing analysis is equivalent to the deployment repeatability analysis for a given EOB with constant member length and backlash. In this chapter, the stiffness of the virtual cable elements at the tensile side was set to 10 times higher than other members. This value is set to avoid numerical instability of the deformation analysis, because the member length difference between a virtual cable element and other members is much larger in comparison with previous examples. The structural analysis was performed under the condition that the three nodes of the bottom surface were fixed.

The distributions of the central point of the top surface triangle were obtained for the three types of friction uncertainties as shown in Fig. 13. It was found that the central point was almost distributed in the shape of an equilateral triangle in all cases. This was different from results of previous studies,[6,7] which showed that the central point was distributed concentrically. In these models, friction uncertainty was not considered. This difference was considered due to the perpendicular friction force

to the shaft axis as shown in Fig. 14.

In addition, the distribution type followed by the friction coefficient did not greatly affect the distribution shape of the central points, because the central points were distributed in the shape of an equilateral triangle in all figures. However, the variation size of the central point was smaller when the truncated normal distribution was used than when the uniform distribution was used. In addition, it became smaller as the standard deviation decrease.

The amount of displacement order of virtual cable elements was about 10^{-3} times as long as the nominal length 0.01 mm. Therefore, the stiffness of the virtual cable element was considered to be set appropriately.

4.2. Effect of the number of stages of EOB

Finally, an effect of the number of stages of EOB on the pointing performance was investigated for repeating the Monte Carlo simulation with 1000 samples. The friction coefficient was assumed to follow a uniform distribution of [-0.57, 0.57] (case 1 in the previous section). The obtained 95-percentile[15] of the pointing direction angle θ_P is shown in Fig. 15. The horizontal and vertical axes indicate a number of stages and the is of distortion angle θ_P, respectively. The value increased as the number of stages increases until 15 stages, where the value was almost fixed with concurrently increasing stages. In addition, the converged value was about 8 arcsec under the trials when only the friction uncertainty was considered. These results show that the friction uncertainty cannot be ignored for the pointing performance requirement of 20 arcsec.

In addition, the validation of Monte Carlo simulation was checked by the standard error of the mean (SEM).[16] SEM is the standard deviation of the mean estimated by samples obtained by Monte Carlo simulation. If SEM is small enough for the mean in 30 stages model which has the largest number of uncertain parameters, it can be concluded that the estimation accuracy of Monte Carlo simulation with 1000 samples is sufficiently high in all models.

Then, the sample mean of θ_P was 4 arcsec, and SEM was 6.7×10^{-2} arcsec in 30 stages model. It means that the mean is in the range of 4 ± 0.2 arcsec with 99.7% possibility. This estimation accuracy is high enough to evaluate the distributions of the central point of the top surface triangle and the relationship between 95-percentile of θ_P and the number of stages. Therefore, the sample size of Monte Carlo simulation (=1000) was considered to be set appropriately.

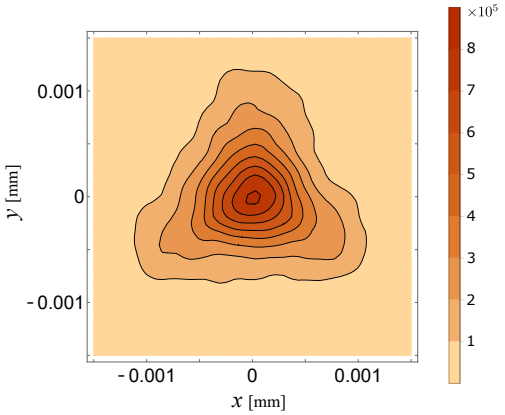

(a) Case 1: U[-0.57, 0.57].

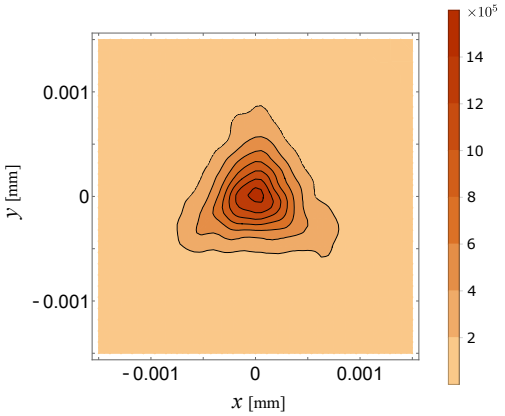

(b) Case 2: $N(0, 0.57/\sqrt{3})$ of [-0.57, 0.57].

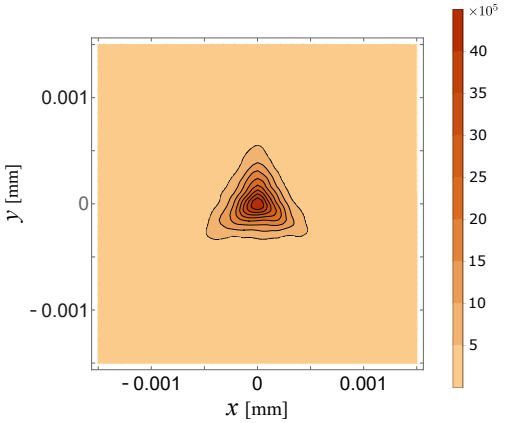

(c) Case 3: $N(0, 0.57/3)$ of [-0.57, 0.57].

Fig. 13. Frequency of position of the central point of the top surface triangle of five-stage EOB model with friction uncertainty by Monte Carlo simulation (sample size: 10000).

5. Conclusion

This study proposes an estimation method for the pointing performance of an extensible optical bench (EOB) considering uncertainty of friction at the connecting nodes. The study builds on the member length uncertainty and the backlash uncertainty of previous research by the same team.

Through numerical calculations, the effect of the uncertainty of the friction force on the deployment repeatability for pointing performance is investigated. It is found that the central point is almost distributed in the shape of an equilateral triangle when the friction coefficient follows both uniform and normal distributions. This study also shows that the 95-percentile of the distortion angle increases until the number of stages reaches 15, when the friction uncertainty is considered. In addition, the 95-percentile value is about 8 arcsec. These results stipulate that the friction uncertainty cannot be ignored for the pointing performance requirement of 20 arcsec.

In the future, it will be necessary to confirm the validity of the proposed friction model with an experiment. The maximum acceptable uncertainty with which to satisfy the required accuracy considering the uncertainties in member length, backlash and friction at connecting nodes should be investigated.

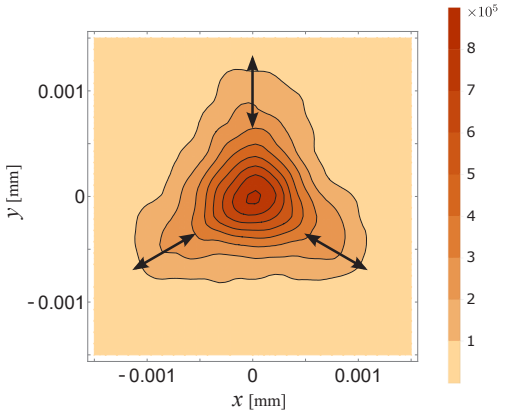

Fig. 14. The directions at right angles to pins.

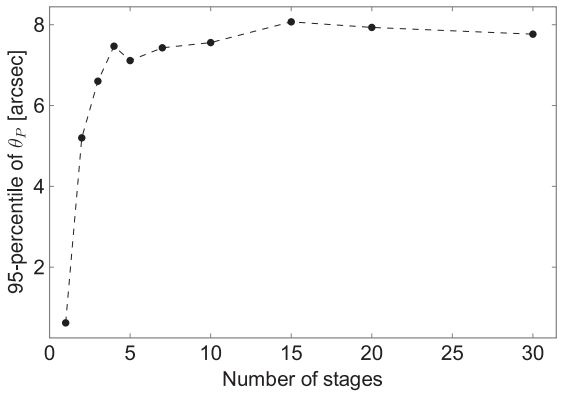

Fig. 15. Relationship between 95-percentile of θ_P and the number of stages.

Acknowledgments

A part of this study was financially supported by a strategic research and development fund of ISAS/JAXA and JSPS KAKENHI 18K18812.

References

1) Funakoshi, Y., Ishimura, K., Hagi, Y., and Iwasa, T.: Application of Preview Information to Pointing Control of Truss Structure Using Artificial Thermal Expansion on Orbit, *J. Intelligent Material Systems and Structures*, **26** (2015), pp. 730-739.
2) Takahashi, T., Kokubun, M., Mitsuda, K., Kelley, R., Ogashi, T., Aharonian, F., et al.: The ASTRO-H (Hitomi) X-ray Astronomy Satellite, *Proc. SPIE*, **9905** (2016), 99050U.
3) Mori, K., Tsuru, T., Nakazawa, K., Ueda, Y., Okajima, T., Murakami, H., et al.: Focusing on Relativistic Universe and Cosmic Evolution: the FORCE mission, XII Multifrequency Behaviour of High Energy Cosmic Sources Workshop, Palermo, Italy, 306-077, 2017.
4) FORCE project group: Focusing on Relativistic Universe and Cosmic Evolution Concept Study Paper, `http://www.cc.miyazaki-u.ac.jp/force/wp-content/uploads/force_proposal.pdf`, 2016 (in Japanese), (accessed February 16, 2018).
5) Puig, L., Barton, A., and Rando, N.: A Review on Large Deployable Structures for Astrophysics Missions, *Acta Astronautica*, **67** (2010), pp. 12-26.
6) Gon, Y. and Kogiso, N.: Pointing Performance Analysis of High-Precision Extensible Optical Bench Considering Member Length Uncertainty, 33rd Space Structure and Material Symposium, Sagamihara, Japan, B15, 2017 (in Japanese).
7) Gon, Y. and Kogiso, N.: Pointing Performance Analysis of High-Precision Extensible Optical Bench Considering Uncertainty of Backlash at Connecting Nodes, 60th JSASS/JSME Structures Conference, Tokushima, Japan, 3B04, 2018 (in Japanese).
8) Gon, Y. and Kogiso, N.: Pointing Performance Analysis of Highly Precise Extensible Optical Bench Considering Uncertainty of Backlash and Friction at Connecting Nodes, 62nd Space Sciences and Technology Conference, Kurume, Japan, 3J16, 2018 (in Japanese).
9) Kitamura, T., Natori, M., Yamashiro, K., and Obata, A.: Development of a High Stiffness Extendible and Retractable Mast 'Himat' for Space Applications, AIAA-90-1054-CP, 1990.
10) Abe, K., Tachikawa, K., Sasaki, T., Kito, A., Yumoto, T., Kurihara, J., et al.: Development of Optical Bench System for ASTRO-H, 57th Space Sciences and Technology Conference, Yonago, Japan, 2D10, 2013 (in Japanese).
11) Yang, T. Y.: *Finite Element Structural Analysis*, Pearson College Div., Englewood Cliffs, 1985.
12) Arora, J. S.: *Introduction to Optimum Design*, 3rd Ed., Academic Press, Waltham, 2011.
13) Baba, M., Kawano, T., and Ishimura, K.: Evaluation of Stiffness Considering Contact Between Longeron and Shaft Parts of Extensible Optical Bench, 32nd Space Structure and Material Symposium, Sagamihara, Japan, A13, 2016 (in Japanese).
14) Grote, K. H. and Feldhusen, J.: *Taschenbuch fur den Maschinenbau*, Springer, London, 1995.
15) Piersol, A. G.: Procedures to Compute Maximum Structural Responses from Predictions or Measurements at Selected Points, *Shock and Vibration*, **3** (1996), pp. 211-221.
16) Minotani, T.: *Statistical Distribution Handbook*, Asakura Publishing, Tokyo, 2003 (in Japanese).